RESEARCH ARTICLE

Performance Analysis of Dual-Hop UAV-Assisted mmWave Links Considering Orientation Fluctuations

RAYYAN AL-KHATAB[1], SAUD ALTHUNIBAT[1,2], (Senior Member, IEEE), ABDULLAH ALHASANAT[1], (Member, IEEE), AND KHALID A. QARAQE[2], (Senior Member, IEEE)

[1]Department of Computer Engineering, Al-Hussein Bin Talal University, Ma'an 71111, Jordan
[2]Department of Electrical and Computer Engineering, Texas A&M University at Qatar, Doha, Qatar

Corresponding author: Saud Althunibat (saud.althunibat@ahu.edu.jo)

ABSTRACT In emergency scenarios, infrastructure of wireless networks is usually damaged and becomes out of service. Therefore, Unmanned Aerial Vehicles (UAVs) have been widely nominated as an alternative to provide prompt and efficient wireless connectivity. To this end, UAV-assisted communication systems are recently being under investigation. In this paper, the focus is on UAV-assisted dual-hop links in which the source, relay and destination can be either ground-based or aerial nodes. Specifically, the paper analyzes the performance of these links in terms of the outage probability (OP) and the bit error rate (BER) considering eight different setups of dual-hop UAV-assisted links operating over the millimeter wave (mmWave) band. Unlike others, the performance analysis is conducted considering practical models of the channel fading, path loss, antennas gain and UAVs' fluctuations. A generalized mathematical framework is followed to obtain the cumulative distribution function (CDF) and the probability density function (pdf) of the overall signal-to-noise ratio (SNR), which are utilized to characterize closed form expressions for the average OP and BER for all proposed setups. Analytical results are validated by Monte Carlo simulations which investigate the role of many setup parameters including the number of antenna elements, the fluctuation intensity, the transmit power and the modulation order. Moreover, results indicate that increasing the number of aerial entities in the link negatively affects its performance due to the impact of the fluctuations on the directional antennas in the mmWave band.

INDEX TERMS Emergency scenarios, unmanned aerial vehicle, relaying systems, millimeter wave, decode-and-forward.

I. INTRODUCTION

An Unmanned Aerial Vehicle (UAV) is a pilot-less aerial vehicle which can be controlled either remotely from a point on the ground or by an onboard computer [1]. This emerging technology has been initially used for various military and security applications such as border surveillance, reconnaissance operations, targeting, monitoring, strike,

The associate editor coordinating the review of this manuscript and approving it for publication was Adao Silva.

airfield security, and battlefield damage assessment [2], [3], [4]. Later on, due to the advances in computing power, artificial intelligence, availability of general purpose software and many other forms of technological advancement, UAVs have been applied in civilian, industrial, public missions and cost effective commercial applications [5], [6], [7], [8], [9], [10], [11].

Among the different UAVs' applications, exploiting UAVs for providing wireless connectivity in emergency scenarios, which include natural disasters, military attacks and public

events [12], has gained an increasing attention. The role of UAVs in such applications is to deploy an efficient and prompt communication system which can provide the desired connectivity [13]. For example, UAVs can be utilized as a flying base stations to assist overloaded ground base stations in congested areas [14]. In addition, UAVs can be employed to build UAV-assisted links to replace damaged terrestrial networks due to natural disasters [15]. It is worth highlighting that communication systems are essential to support emergency management facilities. As rebuilding the destroyed local communication infrastructures may take a long time, it is very necessary a find a suitable alternative to maintain the connectivity between the rescue teams and the affected communities [16]. Therefore, the idea of deploying UAV-assisted links in wireless communication systems has been presented to allow for emergency management teams and relief organizations to establish temporary networks, ensuring seamless communication and coordination during critical times. Additionally, the mobility of UAVs and many other features allow for flexible positioning and adaptive coverage, making them particularly suitable for dynamic emergency scenarios.

One of the main limitations of involving UAVs in communication systems is the continuous UAV's fluctuations as a result of the wind impact or the movement of the internal mechanical motors. Such fluctuations affect the antennas' orientation, which poses a serious challenge for communications systems especially those operating on the millimeter wave (mmWave) band. This is mainly because mmWave-based links are very sensitive to antennas mis-alignment errors that can be casued by UAVs' fluctuations. It is worth mentioning that antennas' misalignment due to orientation fluctuations directly affect the amount of the received power, which is also negatively reflected on other performance aspects including the error performance and outage rate.

Although the performance of UAV-assisted links has been widely investigated in literature, few studies has considered the impact of UAVs' orientation fluctuations. As such, this paper addresses the impact of orientation fluctuations on the performance of UAV-assisted dual-hop mmWave links which are used in emergency scenarios. To this end, eight different setups of UAV-assisted dual-hop links have been considered in which the source, relay and destination can be either aerial or ground node. The performance is characterized in terms of the Outage Probability (OP) and the average Bit Error Rate (BER) at the destination node, taking into account practical models of the channel fading, path loss and antennas gains. Moreover, closed form expressions of both OP and BER are derived following a solid generalized mathematical framework for the eight different system setups considered. Analytical and simulation results are explored to depict the impact of the different configuration parameters, such as the number of antenna elements, fluctuation intensity, transmit power and modulation order, on the performance of the eight different system setups of the dual-hop UAV-assisted

mmWave links. An initial version of this work is included in our previous work [17] which is limited to outage analysis of UAV-assisted links. The contributions of this paper are summarized as follows

- The impact of UAVs' orientation fluctuations on the performance of UAV-assisted mmWave-based dual-hop links is investigated considering practical models of channel fading, path loss and antennas' gains.
- A generalized mathematical framework is presented to characterize both the probability density function (pdf) and the cumulative distribution function (CDF) of the received signal-to-noise ratio (SNR) for eight different setups of the dual-hop UAV-assisted mmWave-based systems.
- Using the developed mathematical framework, closed-form expressions of The end-to-end OP and average BER considering the eight different setups.
- Simulation results are depicted to show the impact of the different operational parameters on both OP and BER. The investigated parameters including the number of antennas elements, fluctuation intensity, transmit power, and modulation order in all different system setups.

The rest of this paper is organized as follows. In Section II, related works are discussed, while the system model is described in Section III, detailing the eight different setups of the dual-hop UAV-assisted systems. Section IV analyzes the performance of the considered system in terms of the end-to-end OP and the average BER. Simulation results are explored and the impact of the different factors are discussed in Section V. Finally, conclusions and future work are drawn in Section VI.

II. RELATED WORKS
Many previous studies have been directed to investigate the performance of UAV-assisted links considering different models of single-hop UAV-assisted links such as Air-to-Ground (AG) [18], [19], Ground-to-Air (GA) [20] and Air-to-Air (AA) [21]. In [18], using Wireless InSite Software, the received signal strength (RSS) and root mean square delay spread (RMS-DS) of multi-path components are analyzed for different UAV heights in AG links considering different environments, such as urban, suburban, rural, and over sea. In [19], real measurements have been obtained for AG channel propagation considering a flying UAV in an open area. In [20], authors provide a method of channel prediction during GA communication to avoid the blockage at 28 GHz. Channel modeling of AA link has been conducted in [21] where Rice model is extended to include multipath effects induced by UAVs' altitude. Other simplified models of GG, GA, AG and AA single-hop links are adopted in [22]. In another work, the performance analysis for a UAV-assisted downlink system using Free Space Optical (FSO) links has been investigated utilizing the Málaga distribution to characterize the effect of atmospheric turbulence in [23].

TABLE 1. Summary of related works.

Work	Dual/single hop	Frequency band	Link setup	Main contributions	Fluctuations considered ?
[18]	single hop	mmWave	AG	RSS analysis using Wireless InSite Software	No
[19]	Single hop	3.1-4.8 GHz	AG	Channel measurements	No
[20]	single hop	mmWave	GA	Channel prediction during G-A blockage	No
[21]	Single-hop	2.4GHz	AA	RSS measurements for channel modelling	No
[22]	Single hop	Up to 5.9 GHz	AG, GA, GG and AA	Channel modelling and connectivity analysis	No
[23]	Single hop	FSO	AG	BER and capacity analysis	No
[25]	Dua-hop A/F	FSO	GAG	OP and BER analysis	No
[26]	Dual-hop D/F	FSO	GAG	OP and BER analysis	No
[27]	Dual-hop D/F	FSO	GAG	Outage analysis and performance optimization	Yes
[28]	Dual hop	mmWave	GAG	Optimal relay location	No
[29]	Dual-hop Full duplex	mmWave	GAG	Optimization and beamform design for sum rate maximization	No
[30]	Dual-hop	Mixed RF/FSO 2GHz	GAG	Ergodic sum rate analysis	Yes (FSO only)
[31]	Dual-hop A/F	mmWave	GAG	Outage analysis	Yes

However, none of these models adopted for single-hop links have considered the antennas' fluctuations caused by UAV(s) vibrations [24].

Dual-hop UAV-assisted links have been proposed as a solution to overcome some of the challenges associated with the single-hop links especially the problem of the limited communication range and blockage. Many works have focused on analysing the performance of dual-hop UAV-assisted links including optimizing the used communication technology (FSO or radio frequency (RF)), the mode of relaying system (one-way relaying or two-way relaying), the relaying protocol (amplify-and-forward (AF) or decode-and-forward(DF)). For example, authors in [25], [26], and [27] present a dual-hop UAV-assisted systems using FSO communication technology. In [25], the performance of the proposed relaying system is studied under the AF relaying protocol while authors in [26] consider the DF relaying protocol. Differently, the impact of antenna orientation has been considered for GAG UAV-assisted link operating on FSO in [27], where the channel distribution is obtained and utilized to obtain the OP.

Other set of works has focused on analysing the mmWave-based dual-hop UAV-assisted systems. In [28], an efficient UAV-relaying method for mmWave-based links is proposed where the UAV gradually adjusts its path to approach the optimal location. In [29], the focus is on optimizing the UAV position, analog beamforming, and power control to maximize the achievable rate in a full-duplex UAV relaying network. To achieve better performance considering different environments, many researches tend to use hybrid systems of RF/FSO, such as [30] that presents the ergodic sum rate analysis of a UAV-based communication system with mixed RF/FSO channels. More related work is reported in [31]

where the pdf and CDF of the SNR are derived for the GAG UAV-assisted dual-hop mmWave-based links considering the UAVs' antennas fluctuations.

In all of the above discussed works (summarized in Table 1), analysis of dual-hop UAV-assisted links have not considered the UAVs' vibrations except [27], [30], [31]. However, works conducted in [27] and [30] consider the impact of the fluctuations on the FSO link, which is different from the RF case. Also, all of these works [27], [30], [31] are limited to the case of GAG setup which represents a special case of UAV-assisted links. To the best of our knowledge, there are no previous works that investigate the impact of the orientation fluctuations of UAV-assisted dual hop mmWave-based links. Therefore, this work comes to complement the research efforts in this direction by analyzing the impact of the orientation fluctuations on the OP and BER.

III. SYSTEM MODEL
A dual-hop communication link is considered in this work, where a source node ($\mathcal{S}$) transmits data towards a destination node ($\mathcal{D}$) via a relay node ($\mathcal{R}$). Being a UAV-assisted link implies that nodes $\mathcal{S}$, $\mathcal{R}$ and $\mathcal{D}$ can be either ground-based or aerial nodes. As such, eight different system setups can be formed by different combinations of aerial and ground nodes, as depicted in Fig. 1, named as AAA, AAG, GAA, GAG, GGG, AGG, GGA and AGA. In all of these notations, the first, second and third letters represent $\mathcal{S}$, $\mathcal{R}$ and $\mathcal{D}$, respectively, where A refers to an aerial node while G refers to a ground node. For example, the AAG setup represents a dual-hop system where $\mathcal{S}$ and $\mathcal{R}$ are both aerial nodes represented by two UAVs while $\mathcal{D}$ is a ground node.
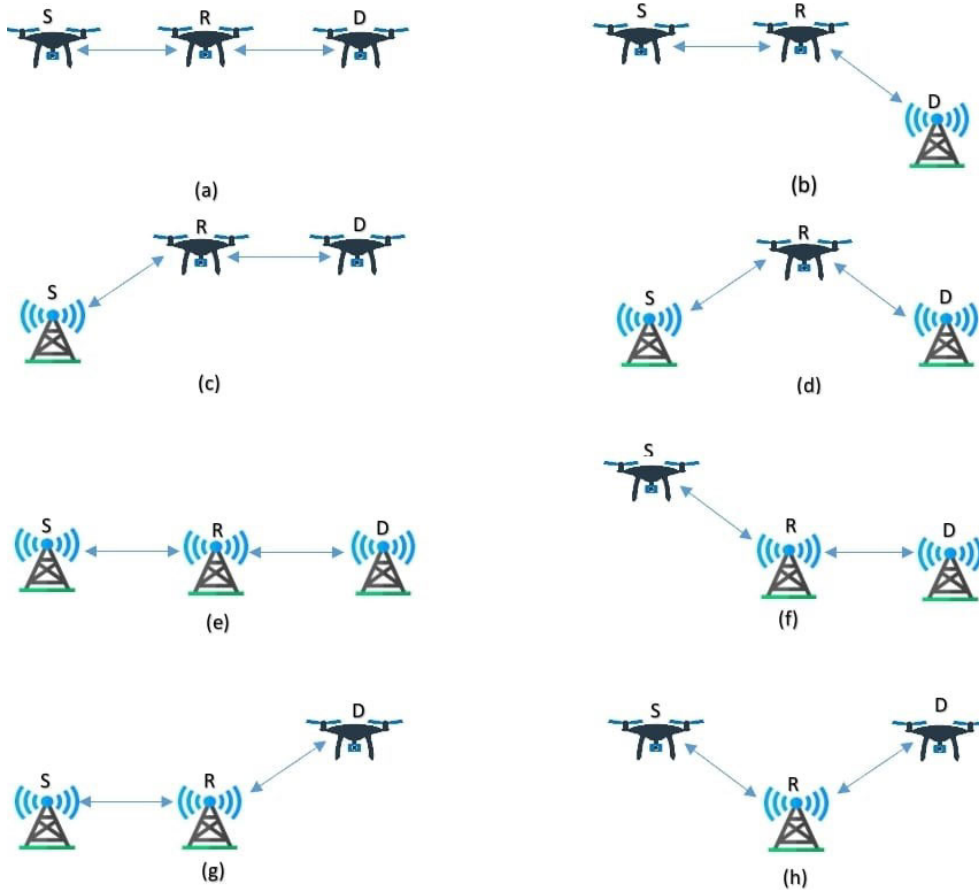
FIGURE 1. The eight different UAV-assisted dual-hop system setups considered: (a) AAA, (b) AAG, (c) GAA, (d) GAG, (e) GGG, (f) AGG, (g) GGA and (h) AGA.

For all setups, the distances on both hops are assumed identical and denoted by L. Also, as the considered link is operating on the mmWave band, directional antennas are utilized at the three nodes. Each of nodes $\mathcal{S}$ and $\mathcal{D}$ is equipped by a single directional antenna to communicate with $\mathcal{R}$, while $\mathcal{R}$ utilizes two directional antennas to communicate with both $\mathcal{S}$ and $\mathcal{D}$ separately.

Our work will start by showing the single-hop studies and equations that introduced in [31] before extending them to the dual-hop relaying system. A general formula of the SNR for a single hop is given as follows:

$$\gamma_{\ell-\ell'} = \frac{P_\ell \, h(L) \, \zeta \, \mathbb{G}_{\ell-\ell'}}{\sigma^2}, \qquad (1)$$

where $\ell - \ell'$ signifies the considered hop ($\mathcal{S} - \mathcal{R}$ or $\mathcal{R} - \mathcal{D}$), ζ is the channel fading power, P_ℓ is the transmit power, $h(L)$ is the path loss, $\mathbb{G}_{\ell-\ell'}$ the overall antennas' gain of the considered link, and σ^2 is the noise power. It is worth to mention here that the transmitted power from all nodes is considered identical and denoted by P. Based on (1), the transmitted signal is affected by channel fading (small-scale propagation effects), path loss (large-scale propagation effects) and antennas' gains. In what follows, we describe the model adopted for each of these effects.

A. PATH LOSS
The adopted model for path loss is based on the recent 3GPP report [32], which expresses the path loss in dB over an aerial distance L, $h_{dB}(L)$, as follows

$$\begin{aligned} h_{dB}(L) = &-20 \log_{10}\left(\frac{40\pi L f_c}{3}\right) \\ &+ \min\{0.03 h_b^{1.73}, 10\} \times \log_{10}(L) \\ &+ \min\{0.044 h_b^{1.73}, 14.77\} - 0.002 \, L \log_{10}(h_b), \end{aligned} \qquad (2)$$

where h_b is the average building height of the area (in meters), and f_c is the carrier frequency. It should be highlighted here that this path loss model is valid for UAV's altitude less than 150m.

B. CHANNEL FADING
Among the different channel fading models, Nakagami fading model has been widely accepted to represent the small-scale channel propagation effects in the mmWave band due to its agreement with real channel measurements [21]. In Nakagami model, the channel power ζ is distributed according to the Gamma distribution. As such, the pdf of ζ is

given as

$$f_\zeta(\zeta) = \frac{m^m \zeta^{m-1}}{\Gamma(m)} \exp(-m\zeta), \quad \zeta > 0, \quad (3)$$

where m is the Nakagami fading parameter and $\Gamma(.)$ is the Gamma function.

C. ANTENNA GAIN

The last variable in the SNR formula (1) is $\mathbb{G}_{\ell-\ell'}$ which represents the gains of the two antennas (transmit and receive antennas) of the considered hop $\ell - \ell'$ (i.e., AA, AG, GA or GG), which is represented by their product, i.e., $\mathbb{G}_{\ell-\ell'} = \mathbb{G}_\ell \mathbb{G}_{\ell'}$. In our work, the antennas are assumed to be uniform square array antennas, each of $N \times N$ elements. The spacing between the elements in both x- and y-directions are set to $\lambda/2$ where λ is the wavelength. Also, the progressive phase shifts in both x and y directions are set to zeros. The gain of the antenna (either transmit or receive antenna) depends on the type of the node carrying the antenna (i.e. either A or G).

1) ANTENNA GAIN OF AERIAL NODES

The radiation gain of a directional antenna is usually represented by the orientation angles of the antenna in x and y directions, denoted by $\phi_{\ell x}$ and $\phi_{\ell y}$, respectively. From the 3GPP report [32], the angles, $\phi_{\ell x}$ and $\phi_{\ell y}$, are combined to form other two angles denoted by ϕ_ℓ and φ_ℓ and expressed as follows

$$\phi_\ell = \tan^{-1} \sqrt{\sin^2(\phi_{\ell x}) + \sin^2(\phi_{\ell y})},$$
$$\varphi_\ell = \tan^{-1}\left(\frac{\sin(\phi_{\ell y})}{\sin(\phi_{\ell x})}\right). \quad (4)$$

For an aerial node, both $\phi_{\ell x}$ and $\phi_{\ell y}$ are actually random as a result of the random hovering vibrations. As such, both angles are assumed to be Gaussian distributed, i.e. $\phi_{\ell x} \sim N(\phi'_{\ell x}, \sigma^2_{\ell o})$ and $\phi_{\ell y} \sim N(\phi'_{\ell y}, \sigma^2_{\ell o})$. Based on [33], the array radiation gain is expressed as follows

$$\mathbb{G}_\ell(\phi_{\ell x}, \phi_{\ell y}) = \mathcal{G}_0(N_\ell)\mathcal{G}_a(\phi_{\ell x}, \phi_{\ell y})\mathcal{G}_e(\phi_{\ell x}, \phi_{\ell y}), \quad (5)$$

where $\mathcal{G}_a$ is an array factor, $\mathcal{G}_e$ is the single element radiation pattern and $\mathcal{G}_0$ is a constant defined later. From the 3GPP, the single element radiation pattern, $G_{e,3dB} = 10 \times \log_{10}(\mathcal{G}_e)$ of each single antenna element is obtained as follows

$$G_{e3dB} = G_{max} - \min\left\{-(G_{e3dB,1} + G_{e3dB,2}), F_m\right\},$$
$$G_{e3dB,1} = -\min\left\{12\left(\frac{\phi_e - 90}{\phi_{e3dB}}\right)^2, G_{SL}\right\},$$
$$G_{e3dB,2} = -\min\left\{12\left(\frac{\varphi_\ell}{\varphi_{e3dB}}, F_m\right)\right\},$$
$$\phi_e = \tan^{-1}\left(\frac{\sqrt{1 + \sin^2(\phi_{\ell x})}}{\sin(\phi_{\ell y})}\right), \quad (6)$$

where $\phi_{e3dB} = 65$ and $\varphi_{e3dB} = 65$ are the vertical and horizontal 3D beam waves, respectively, $G_{max} = 8$ dBi is the maximum directional gain of the antenna element,

$F_m = 30dB$ is the front-back ratio, and $G_{SL} = 30$ dB is the side-lobe level limit. The array factor $\mathcal{G}_a(\phi_{\ell x}, \phi_{\ell y})$ for a square array of N^2 elements can be obtained as follows

$$\mathcal{G}_a(\phi_{\ell x}, \phi_{\ell y}) = \left(\frac{\sin\left(\frac{N(\pi \sin\phi_\ell \cos\varphi_\ell)}{2}\right)}{N \sin\left(\frac{\pi \sin\phi_\ell \cos\phi_\ell}{2}\right)}\right)^2$$
$$\times \left(\frac{\sin\left(\frac{N(\pi \sin\phi_\ell \sin\varphi_\ell)}{2}\right)}{N \sin\left(\frac{\pi \sin\phi_\ell \sin\varphi_\ell}{2}\right)}\right)^2. \quad (7)$$

Finally, $\mathcal{G}_0$ is computed utilizing the relation below which ensures that the radiated power from transmit antennas is kept the same:

$$\mathcal{G}_0(N) = \frac{1}{\int_0^\pi \int_0^{2\pi} \mathcal{G}_a(\phi_\ell, \varphi_\ell)\mathcal{G}_e(\phi_\ell, \varphi_\ell) \sin(\phi_\ell)d\phi_\ell d\varphi_\ell} \quad (8)$$

More details on the element and array radiation pattern are provided in [33] and [34].

2) ANTENNA GAIN FOR GROUND NODES

Unlike the aerial node, the directional antenna installed at a ground node can be considered in a perfect alignment as it is not affected by fluctuations. Therefore, the antenna gain at a ground node can be computed using the same procedure followed for the aerial node while assuming $\phi_{\ell x} \simeq 0$ and $\phi_{\ell y} \simeq 0$, as follows

$$\mathbb{G}_{t,max} = \mathbb{G}_\ell(\phi_{\ell x} \simeq 0, \phi_{\ell y} \simeq 0) \quad (9)$$

IV. SYSTEM PERFORMANCE ANALYSIS

In this section, the performance of dual-hop cooperative links of the considered setups is analyzed by quantifying two important metrics: the end-to-end OP and the average BER.

A. OP ANALYSIS

In general, OP is the probability that the channel capacity falls below a predefined threshold (C_{th}), which is mathematically expressed as follows

$$\mathbb{P}_{out} = \Pr\{\log_2(1 + \gamma) \leq C_{th}\}, \quad (10)$$

or simply, OP can be defined as the probability that the SNR γ falls below a predefined threshold γ_{th} as follows

$$\mathbb{P}_{out} = \Pr\{\gamma \leq \gamma_{th}\}. \quad (11)$$

For a dual-hop systems, the OP is defined as the probability that the SNR of any of the two hops, i.e., $\mathcal{S} - \mathcal{R}$ or $\mathcal{R} - \mathcal{D}$, falls below the outage threshold γ_{th}. Therefore, $\mathbb{P}_{out}$ can be expressed as follows

$$\mathbb{P}_{out} = \Pr\{\min\{\gamma_1, \gamma_2\} \leq \gamma_{th}\}, \quad (12)$$

where γ_1 and γ_2 represent the SNR of the $\mathcal{S} - \mathcal{R}$ hop and the $\mathcal{R} - \mathcal{D}$ hop, respectively, of the considered dual-hop system. Let us define $\gamma_{min} = \min\{\gamma_1, \gamma_2\}$. Therefore, The end-to-end OP can be rewritten as follows:

$$\mathbb{P}_{out} = \Pr\{\gamma_{min} \leq \gamma_{th}\} = F_{\gamma_{min}}(\gamma_{th}), \quad (13)$$

where $F_{\gamma_{min}}(\gamma)$ is the CDF of γ_{min}, which can be expressed as follows [35]:

$$F_{\gamma_{min}}(\gamma) = F_{\gamma_1}(\gamma) + F_{\gamma_2}(\gamma) - F_{\gamma_1}(\gamma) * F_{\gamma_2}(\gamma), \quad (14)$$

where $F_{\gamma_1}(\gamma)$ and $F_{\gamma_2}(\gamma)$ represent the CDFs of the $\mathcal{S} - \mathcal{R}$ hop and the $\mathcal{R} - \mathcal{D}$ hop, respectively. Given the different channel effects encountered in different link types (i.e., AA, AG, GA, or GG) in the two hops, the CDF of each hop should follow the link type. In [31], three different closed form expressions of the CDFs of AA, AG and GA links, have been derived. Next, we will unify the representation of these CDFs in one generalized function that accommodate all of these link types and the GG link as well. Specifically, the CDF of the hop $\ell - \ell'$ can be expressed as follows:

$$F_{\gamma_{\ell-\ell'}}(\gamma) = \sum_{i_\ell=0}^{2T_\ell-1} \sum_{j_{\ell'}=0}^{2T_{\ell'}-1} \frac{\mathbb{J}_{i_\ell}^\ell \ \mathbb{J}_{j_{\ell'}}^{\ell'}}{\Gamma(m)} \times \nu\left(m, \mu_{i_\ell,j_{\ell'}}^{\ell-\ell'} \gamma\right) \quad (15)$$

where $\nu(.,.)$ is the lower incomplete gamma function, and $\mathbb{J}_i^\ell$ is defined as follows:

$$\mathbb{J}_{i_\ell}^\ell = \begin{cases} M\left(\dfrac{\phi'_{\ell,xy}}{\sigma_{\ell o}}, \dfrac{i_\ell}{T_\ell N \sigma_{\ell o}}\right) - M\left(\dfrac{\phi'_{\ell,xy}}{\sigma_{\ell o}}, \dfrac{i_\ell+1}{T_\ell N \sigma_{\ell o}}\right), \\ \qquad \text{if } \ell \equiv A \\ 1, \quad \text{if } \ell \equiv G, \end{cases}$$

$$(16)$$

where $M(.,.)$ the Marcum Q-function. The function $\mathbb{J}_{j_{\ell'}}^{\ell'}$ can be computed by the same formula of $\mathbb{J}_{i_\ell}^\ell$ with replacing i_ℓ and ℓ by $j_{\ell'}$ and ℓ'. The value of the parameter T_ℓ is substituted as follows:

$$T_\ell = \begin{cases} 40, & \ell \equiv A, \\ \dfrac{1}{2}, & \ell \equiv G \end{cases}, \quad (17)$$

and $T_{\ell'}$ is computed using the same formula by replacing ℓ by ℓ'. The variable $\mu_{i_\ell,j_{\ell'}}^{\ell-\ell'}$ is expressed as follows:

$$\mu_{i_\ell,j_{\ell'}}^{\ell-\ell'} = \frac{m\sigma^2}{Ph(L)\mathbb{R}_{i_\ell,j_{\ell'}}^{\ell-\ell'}}, \quad (18)$$

where $\mathbb{R}_{i_\ell,j_{\ell'}}^{\ell-\ell'}$ is given in (19), as shown at the bottom of the next page, where $\mathbb{G}_0''(N)$ is given as follows:

$$\mathbb{G}_0''(N) = 0.2025 \times 10^{\frac{Gmax}{10}} \mathcal{G}_o(N). \quad (20)$$

Finally, the OP of any of the considered eight setups can be expressed by substituting the proper CDFs corresponding to the considered setup in (14). For example, the OP of the AGA system setup can be computed by replacing F_{γ_1} and F_{γ_2} by the CDFs $F_{A-G}(\gamma_{th})$ and $F_{G-A}(\gamma_{th})$ in (14), which leads to the OP of the AGA system setup as depicted in (21), as shown at the bottom of the next page. OP formulas of other setups can be obtained in a similar procedure.

B. BER ANALYSIS

The average BER is another important performance metric for wireless communication systems. In our considered dual-hop UAV-assisted communication setups, it is clear that the BER at $\mathcal{S}$ and $\mathcal{D}$ nodes are identical in all proposed setups. Hence, the BER analysis can be calculated at just one node, say $\mathcal{D}$. Consider the bit block transmitted from $\mathcal{S}$ is denoted by $\mathbf{b}$, received at $\mathcal{R}$ as $\hat{\mathbf{b}}$, and finally received at $\mathcal{D}$ as $\hat{\hat{\mathbf{b}}}$. Therefore, the average BER at $\mathcal{D}$, denoted by $\text{BER}_{\mathcal{SD}}$, can be expressed as

$$\text{BER}_{\mathcal{SD}} = \text{Pr}.(\hat{\hat{b}} \neq b). \quad (22)$$

By substituting e_{SR} and e_{RD} that represent error vectors in the data transmitted from node $\mathcal{S}$ to node $\mathcal{R}$ and from node $\mathcal{R}$ to node $\mathcal{D}$, respectively, the equation can be rewritten as follows

$$\begin{aligned} \text{BER}_{\mathcal{SD}} &= \text{Pr}.(\hat{b} \oplus e_{RD} \neq b) \\ &= \text{Pr}.(b \oplus e_{SR} \oplus e_{RD} \neq b) \\ &= \text{Pr}.(e_{SR} \oplus e_{RD} \neq 0). \end{aligned} \quad (23)$$

The last line of (23) states that the event $e_{\mathcal{SR}} \oplus e_{\mathcal{RD}} \neq 0$ occurs only when the bits in the error vectors. This case can be further expanded due to the fact the two hops are independent as follows:

$$\begin{aligned} \text{BER}_{\mathcal{SD}} &= \text{Pr}.(e_{SR} = 1 \cap e_{RD} = 0) \\ &+ \text{Pr}.(e_{SR} = 0 \cap e_{RD} = 1). \end{aligned} \quad (24)$$

As $e_{\mathcal{SR}}$ and $e_{\mathcal{RD}}$ are two independent error events [35], (24) can be simplified as follows:

$$\begin{aligned} \text{BER}_{\mathcal{SD}} &= \text{Pr}.(e_{SR} = 1)\text{Pr}.(e_{RD} = 0) \\ &+ \text{Pr}.(e_{SR} = 0)\text{Pr}.(e_{RD} = 1), \end{aligned} \quad (25)$$

which can be rewritten as follows

$$\text{BER}_{\mathcal{SD}} = \alpha_{\mathcal{S}-\mathcal{R}} + \alpha_{\mathcal{R}-\mathcal{D}} - 2\alpha_{\mathcal{S}-\mathcal{R}}\alpha_{\mathcal{R}-\mathcal{D}}, \quad (26)$$

where $\alpha_{\mathcal{S}-\mathcal{R}}$ and $\alpha_{\mathcal{R}-\mathcal{D}}$ represent the BER in the link $\mathcal{S} - \mathcal{R}$ and $\mathcal{R} - \mathcal{D}$, respectively. For a coherent PSK modulation scheme, the average BER over a fading channel for the link $\ell - \ell'$ can be expressed as follows [36]:

$$\alpha_{\ell-\ell'} = \frac{\delta}{2} \int_0^\infty \left(1 - \text{erf}(\sqrt{\overline{\omega}\gamma_{\ell-\ell'}})\right) f_{\gamma_{\ell-\ell'}}(\gamma) \, d\gamma_{\ell-\ell'}, \quad (27)$$

where $\text{erf}(\cdot)$ is the error function, γ, while δ, and $\overline{\omega}$ can be determined respectively as follows:

$$\delta = \begin{cases} 1, & \text{if } M = 2 \\ \dfrac{2}{\log_2 M}, & \text{if } M > 2 \end{cases}. \quad (28)$$

$$\overline{\omega} = \begin{cases} 1, & \text{if } M = 2 \\ \sin^2(\dfrac{\pi}{M}), & \text{if } M > 2 \end{cases}. \quad (29)$$

The pdf $f_{\gamma_{\ell-\ell'}}(\gamma)$ is the probability density function of γ_{th} at $\ell - \ell'$ and it can be computed as follow:

$$
f_{\gamma_{\ell-\ell'}}(\gamma) = \sum_{i_\ell=0}^{2T_\ell-1} \sum_{j_{\ell'}=0}^{2T_{\ell'}-1} \frac{\mathbb{J}_{i_\ell}^\ell \, \mathbb{J}_{j_{\ell'}}^{\ell'}}{\Gamma(m)} \mu_{i_\ell,j_{\ell'}}^{\ell-\ell'} \gamma^{m-1}
$$
$$
\times \exp\left(m, \mu_{i_\ell,j_{\ell'}}^{\ell-\ell'} \, \gamma\right). \tag{30}
$$

Accordingly, (27) can be rewritten as follows:

$$
\alpha_{\ell-\ell'}
$$
$$
= \frac{\delta}{2}\Bigg(1 - \sum_{i_\ell=0}^{2T_\ell-1} \sum_{j_{\ell'}=0}^{2T_{\ell'}-1} \frac{\mathbb{J}_{i_\ell}^\ell \, \mathbb{J}_{j_{\ell'}}^{\ell'}}{\Gamma(m)} \mu_{i_\ell,j_{\ell'}}^{\ell-\ell'}
$$
$$
\times \int_0^\infty \mathrm{erf}\left(\sqrt{\overline{\omega}\gamma_{\ell-\ell'}}\right) \gamma^{m-1} \exp\left(-\mu_{i_\ell,j_{\ell'}}^{\ell-\ell'} \, \gamma\right) \cdot d\gamma_{\ell-\ell'}\Bigg). \tag{31}
$$

By solving the integral in (31) [37, eq.4.3.8], $\alpha_{\ell-\ell'}$ can be expressed in a closed from expression as follow:

$$
\alpha_{\ell-\ell'} = \frac{\delta}{2}\Bigg(1 - 2\sum_{i_\ell=0}^{2T_\ell-1} \sum_{j_{\ell'}=0}^{2T_{\ell'}-1} \sqrt{\frac{\overline{\omega}}{\pi}} \left(\mu_{i_\ell,j_{\ell'}}^{\ell-\ell'}\right)^{\frac{-2m-1}{2}}
$$

TABLE 2. Simulation parameters.

Parameter	Value	Parameter	Value
f_c	50 GHz	N	$\{4, 8, 12\}$
h_b	30 m	m	3
σ^2	-110 dBm	L	1000 m
P	20 dBm	σ_o^2	$\{1^o, 3^o, 5^o\}$
G_{max}	8 dBm	M	$\{2, 4, 8\}$

$$
\Gamma\left(\frac{2m+1}{2}\right) {}_2F_1\left(\frac{1}{2}, \frac{2m+1}{2}; \frac{3}{2}; -\frac{\sin^2(\frac{\pi}{M})}{\mu_{i_\ell,j_{\ell'}}^{\ell-\ell'}}\right)\Bigg), \tag{32}
$$

where ${}_2F_1(., .; .)$ is the hyber-geometric Gauss function. Finally, the average BER$_{\mathcal{SD}}$ can be obtained by substituting $\alpha_{\ell-\ell'}$ from (32) for both links in (26).

V. SIMULATION RESULTS

In this section, the results of Monte Carlo simulation for our proposed dual-hop UAV-assisted mmWave system setups in terms of the two metrics; the end-to-end OP and the average BER are explored and discussed. A set of simulation parameters are set to fixed values which are listed in Table 2. Results are explored in figures for the system setups

$$
\mathbb{R}_{i_\ell,j_{\ell'}}^{\ell-\ell'} =
\begin{cases}
4\pi^4 \left(\mathbb{G}_0''(N)\right)^2, & \text{if } i_\ell = j_{\ell'} = 0 \ \& \ \ell - \ell' \equiv A - A \\[2mm]
2\pi^2 \left(\mathbb{G}_0''(N)\right)^2 \dfrac{T_\ell^2 \sin^2\left(\frac{i_\ell \pi}{T_\ell}\right)}{i_\ell^2}, & \text{if } i_\ell \neq 0 \ \& \ j_{\ell'} = 0 \ \& \ \ell - \ell' \equiv A - A \\[2mm]
2\pi^2 \left(\mathbb{G}_0''(N)\right)^2 \dfrac{T_{\ell'}^2 \sin^2\left(\frac{j_{\ell'} \pi}{T_{\ell'}}\right)}{j_{\ell'}^2}, & \text{if } i_\ell = 0 \ \& \ j_{\ell'} \neq 0 \ \& \ \ell - \ell' \equiv A - A \\[2mm]
4 \left(\mathbb{G}_0''(N)\right)^2 \dfrac{T_\ell^2 T_{\ell'}^2 \sin^2\left(\frac{i_\ell \pi}{T_\ell}\right) \sin^2\left(\frac{j_{\ell'} \pi}{T_{\ell'}}\right)}{i_\ell^2 j_{\ell'}^2}, & \text{if } i_\ell \neq 0 \ \& \ j_{\ell'} \neq 0 \ \& \ \ell - \ell' \equiv A - A \\[2mm]
2\pi^2 \mathbb{G}_{t,max} \mathbb{G}_0''(N), & \text{if } i_\ell = 0 \ \& \ \ell - \ell' \equiv A - G \\[2mm]
\mathbb{G}_{tmax} \mathbb{G}_0''(N) \dfrac{T_\ell^2 \sin^2\left(\frac{i_\ell \pi}{T_\ell}\right)}{i_\ell^2}, & \text{if } i_\ell \neq 0 \ \& \ \ell - \ell' \equiv A - G \\[2mm]
2\pi^2 \mathbb{G}_{t,max} \mathbb{G}_0''(N), & \text{if } j_{\ell'} = 0 \ \& \ \ell - \ell' \equiv G - A \\[2mm]
\mathbb{G}_{t,max} \mathbb{G}_0''(N) \dfrac{T_{\ell'}^2 \sin^2\left(\frac{j_{\ell'} \pi}{T_{\ell'}}\right)}{j_{\ell'}^2}, & \text{if } j_{\ell'} \neq 0 \ \& \ \ell - \ell' \equiv G - A \\[2mm]
\left(\mathbb{G}_{t,max}\right)^2, & \text{if } \ell - \ell' \equiv G - G
\end{cases}
\tag{19}
$$

$$
\mathbb{P}_{out}^{AGA} = F_{\gamma_{A-G}}(\gamma_{th}) + F_{\gamma_{G-A}}(\gamma_{th}) - F_{\gamma_{A-G}}(\gamma_{th})F_{\gamma_{G-A}}(\gamma_{th})
$$
$$
= \sum_{i_A=0}^{2T_A-1} \sum_{j_G=0}^{2T_G-1} \frac{\mathbb{J}_{i_A}^A \, \mathbb{J}_{j_G}^G}{\Gamma(m)} \times \nu\left(m, \mu_{i_A,j_G}^{A-G} \, \gamma_{th}\right) + \sum_{i_G=0}^{2T_G-1} \sum_{j_A=0}^{2T_A-1} \frac{\mathbb{J}_{i_G}^G \, \mathbb{J}_{j_A}^A}{\Gamma(m)} \times \nu\left(m, \mu_{i_G,j_A}^{G-A} \, \gamma_{th}\right)
$$
$$
- \sum_{i_A=0}^{2T_A-1} \sum_{j_G=0}^{2T_G-1} \frac{\mathbb{J}_{i_A}^A \, \mathbb{J}_{j_G}^G}{\Gamma(m)} \times \nu\left(m, \mu_{i_A,j_G}^{A-G} \, \gamma_{th}\right) \times \sum_{i_G=0}^{2T_G-1} \sum_{j_A=0}^{2T_A-1} \frac{\mathbb{J}_{i_G}^G \, \mathbb{J}_{j_A}^A}{\Gamma(m)} \times \nu\left(m, \mu_{i_G,j_A}^{G-A} \, \gamma_{th}\right) \tag{21}
$$

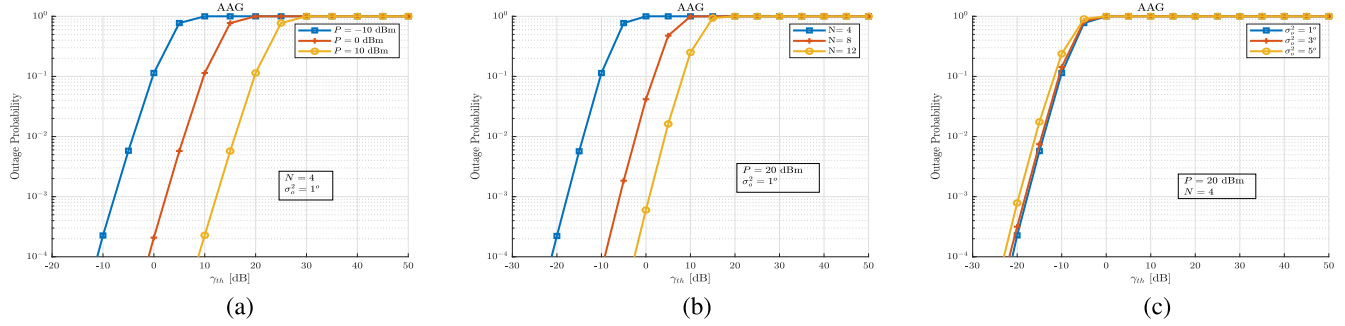**FIGURE 2.** The end-to-end OP of the AAG setup versus γ_{th} showing (a) The impact of P (b) The impact of N and (c) The impact of σ_o^2.
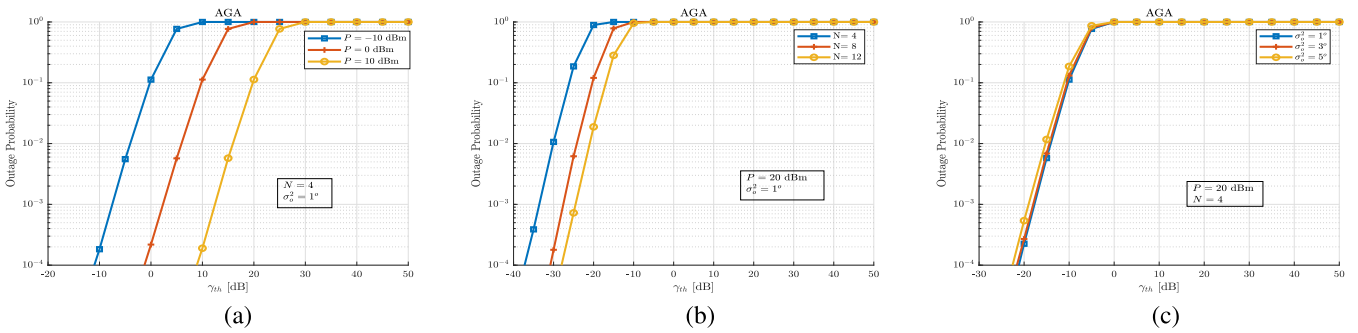

FIGURE 3. The end-to-end OP of the AGA setup versus γ_{th} showing (a) The impact of P (b) The impact of N and (c) The impact of σ_o^2.
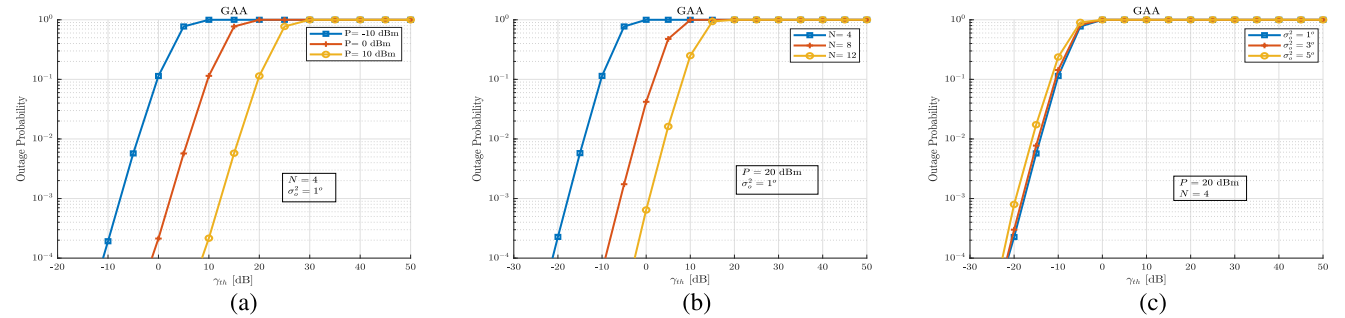

FIGURE 4. The end-to-end OP of the GAA setup versus γ_{th} showing (a) The impact of P (b) The impact of N and (c) The impact of σ_o^2.

AAG, AGA, GAA, GGA, AGG, GAG, AAA, and GGG, respectively, in the following subsections.

A. OP RESULTS

In this subsection, the end-to-end OP (P_{out}) versus γ_{th} is explored in Fig. 2 to Fig. 9 for all setups considered. Each of these figures includes three sub-figures that investigate the impact of the transmit power P, the number of antenna elements N and the UAV's vibration intensity σ_o^2. In the first sub-figures (a) in Fig. 2 - Fig. 9, N and σ_o^2 are fixed to $N = 4$ and $\sigma_0^2 = 1°$, respectively, while three different values of the transmit power P are assumed $P = -10$, 0 and 10 dBm. From these results, the impact of transmit power can be clearly observed, where the increase in transmit power reduces the OP. For example, at $\gamma_{th} = 10$ dB for AAG

setup, OP is decreased from 10^{-1} to 10^{-4} when the transmit power increases from 0 to 10 dB. The same behaviour can be observed in all other setups, which is mainly due to the increase of the received signal power as the transmit power increases.

In the second sub-figures in all figures (i.e., sub-figures (b) in Fig. 2 - Fig. 9), the impact of varying the number of antenna elements on the OP is depicted. To this end, both P and σ_o^2 are fixed to $P = 20$dBm and $\sigma_o^2 = 1°$, respectively, while three different values of the number of antenna elements N are assumed $N = 4$, 8 and 12. It is worth mentioning that all entities in all setups are equipped by identical antenna type and size. Based on these results, it can be realized that increasing the number of antenna elements N at each entity will reduce the OP. This can be referred to the fact that increasing the antenna elements will improve the received
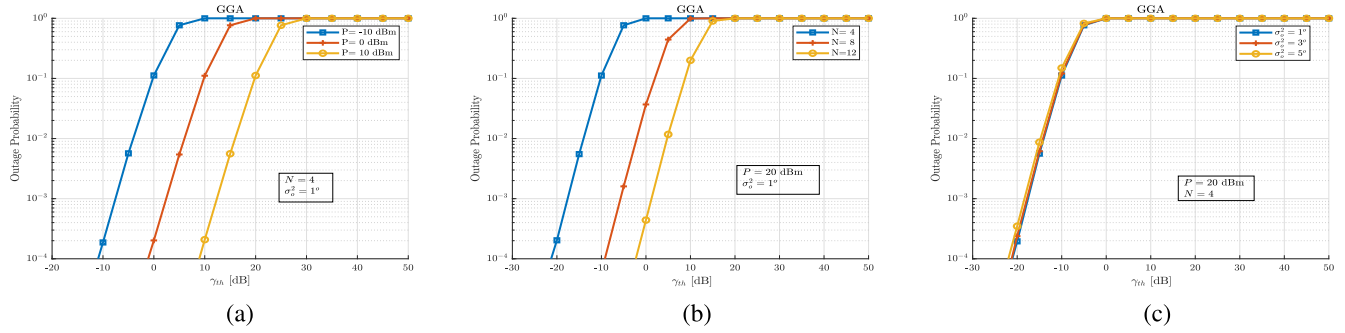
FIGURE 5. The end-to-end OP of the GGA setup versus γ_{th} showing (a) The impact of P (b) The impact of N and (c) The impact of σ_o^2.
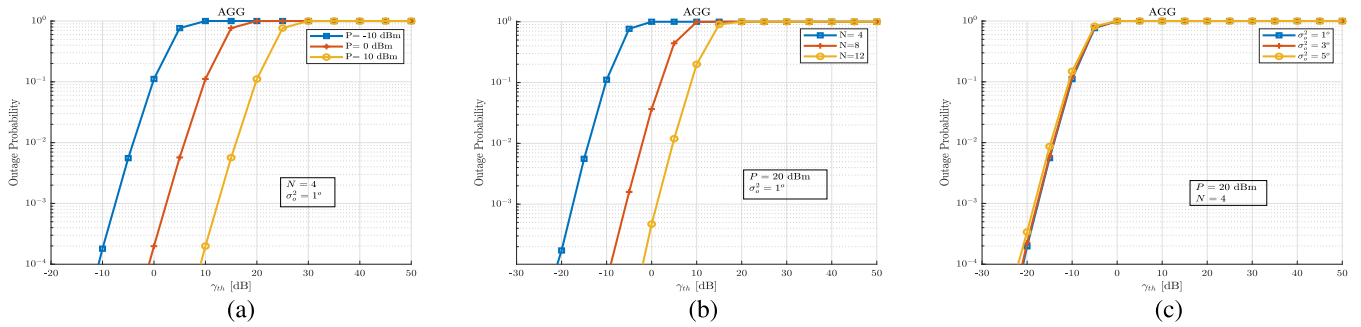

FIGURE 6. The end-to-end OP of the AGG setup versus γ_{th} showing (a) The impact of P (b) The impact of N and (c) The impact of σ_o^2.
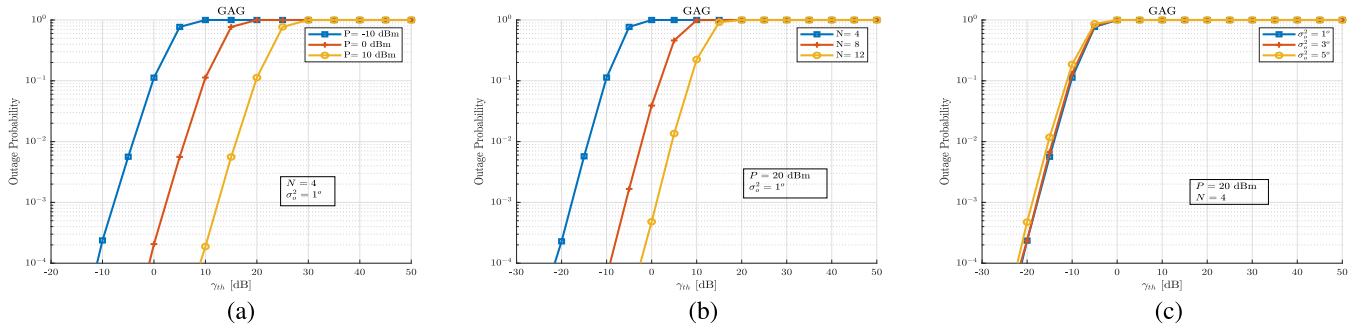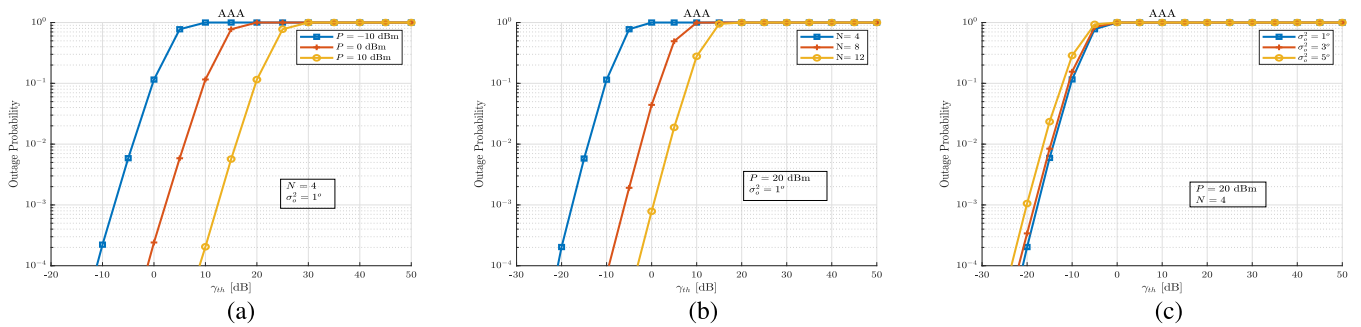

FIGURE 7. The end-to-end OP of the GAG setup versus γ_{th} showing (a) The impact of P (b) The impact of N and (c) The impact of σ_o^2.

FIGURE 8. The end-to-end OP of the AAA setup versus γ_{th} showing (a) The impact of P (b) The impact of N and (c) The impact of σ_o^2.

SNR at each hop, and thus, the link outage will be reduced, as depicted in all setups with different extents.

The last set of OP results are included in the third sub-figures (c) in Fig. 2 - Fig. 9, which are dedicated to show
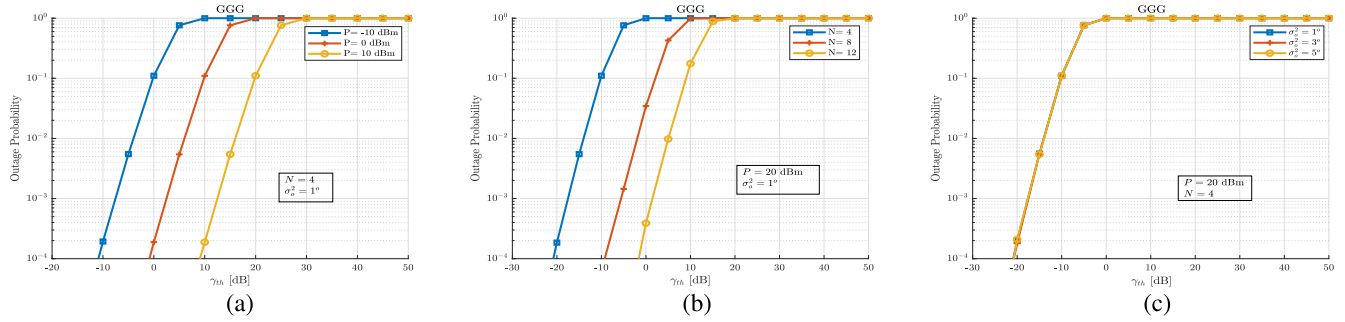
FIGURE 9. The end-to-end OP of the GGG setup versus γ_{th} showing (a) The impact of P (b) The impact of N and (c) The impact of σ_o^2.
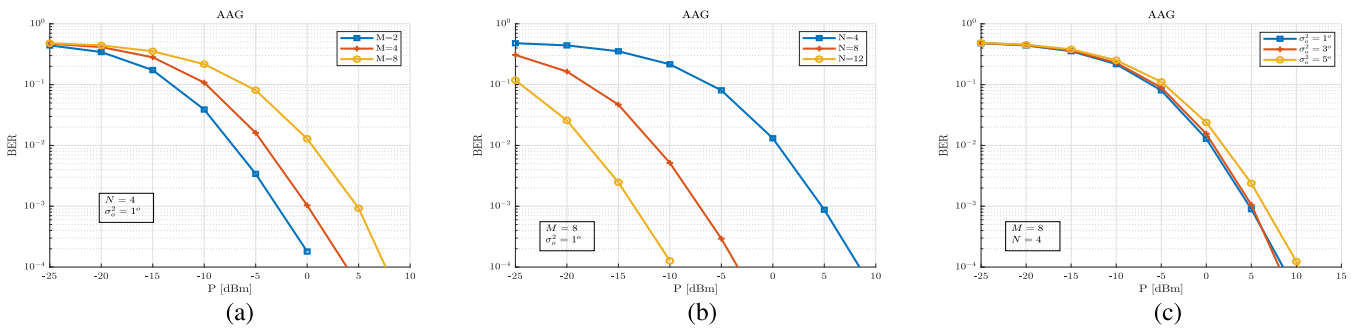

FIGURE 10. The BER of the AAG setup versus the transmit power showing (a) The impact of M (b) The impact of N and (c) The impact of σ_o^2.
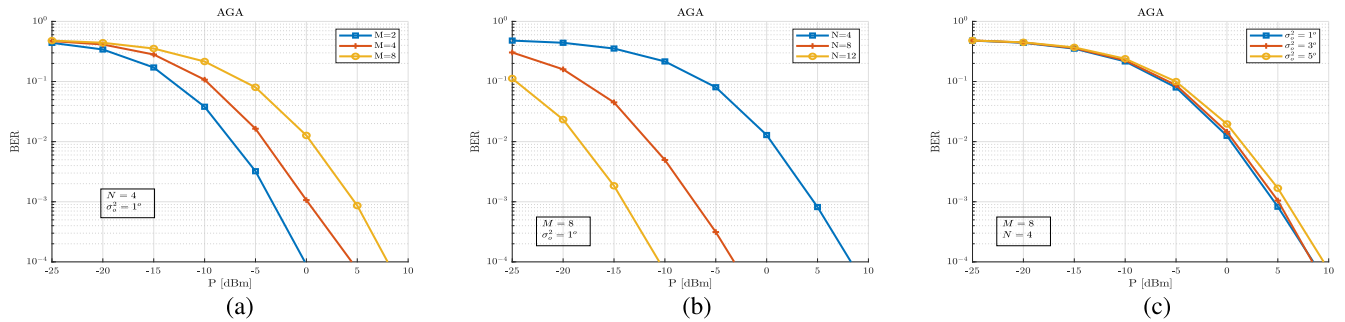

FIGURE 11. The BER of the AGA setup versus the transmit power showing (a) The impact of M (b) The impact of N and (c) The impact of σ_o^2.
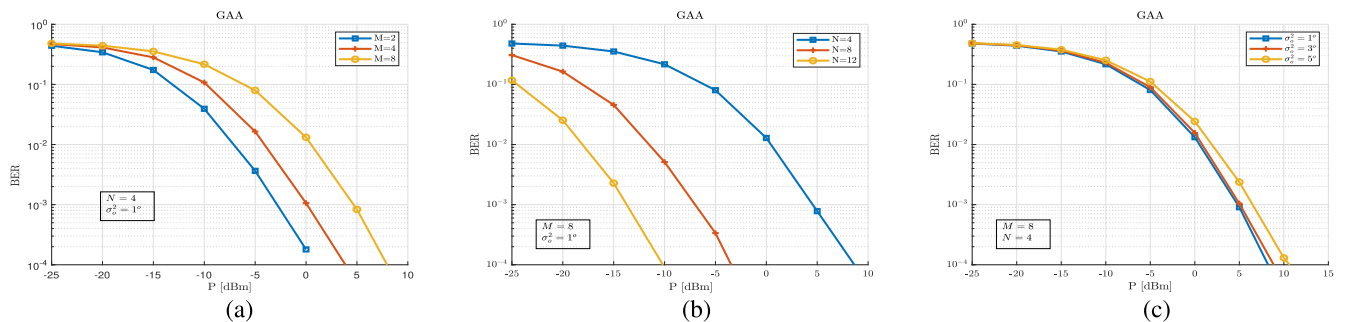

FIGURE 12. The BER of the GAA setup versus the transmit power showing (a) The impact of M (b) The impact of N and (c) The impact of σ_o^2.

the impact of the vibration intensity σ_o^2 on the OP for all setups. To this end, both the N and P are fixed to $N = 4$ and $P = 20$ dBm, respectively, while three different values of the vibration intensity σ_o^2 are assumed $\sigma_o^2 = 1°$, $3°$ and $5°$. It

is clear that increasing the vibration intensity has a negative impact represented by increasing the OP for all system setups (except for the GGG system setup). This is mainly because of UAVs' vibration will contribute to waste some of the transmit
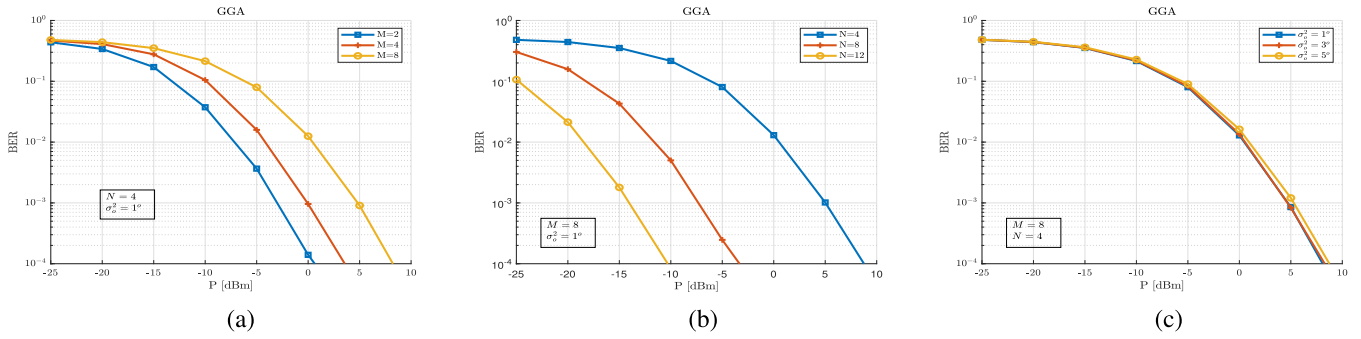
FIGURE 13. The BER of the GGA setup versus the transmit power showing (a) The impact of M (b) The impact of N and (c) The impact of σ_o^2.
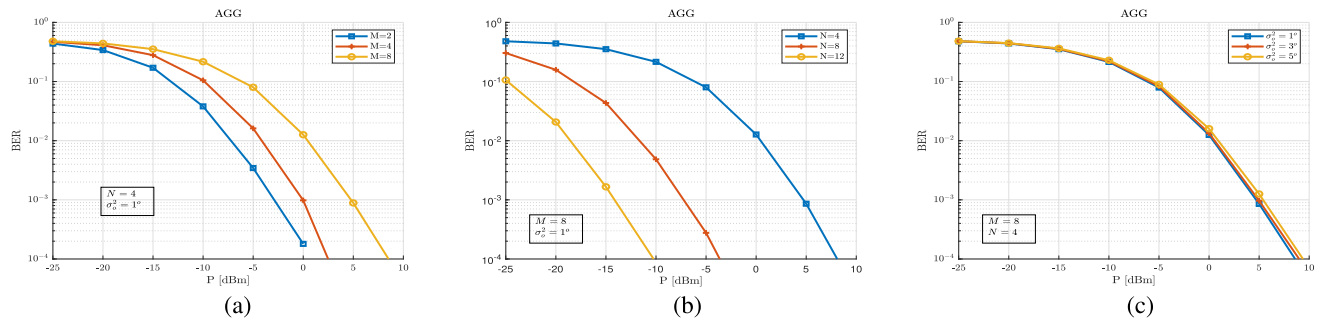

FIGURE 14. The BER of the AGG setup versus the transmit power showing (a) The impact of M (b) The impact of N and (c) The impact of σ_o^2.
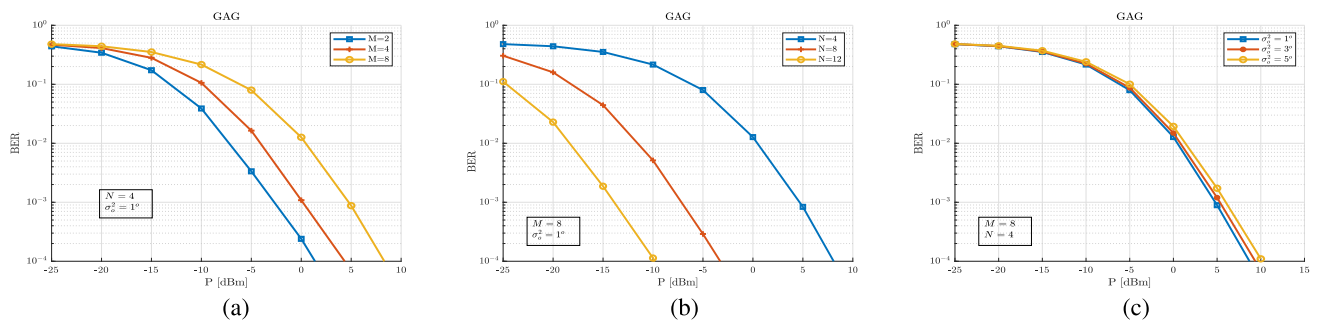

FIGURE 15. The BER of the GAG setup versus the transmit power showing (a) The impact of M (b) The impact of N and (c) The impact of σ_o^2.

power which will not reach the receiver. As such, the amount of the received power will be reduced, and hence, the OP will increase. It is worth mentioning that vibration intensity has no impact in the GGG setup (Fig. 9-(c)) as no UAVs are involved in this setup.

B. BER RESULTS
The BER results for all setups considered are depicted in Fig. 10-Fig. 17, with the same order of OP results. A general observation can be noted in all BER figures is that the average BER decreases as the transmit power increases. This common behaviour between all investigated setups is mainly because increasing the transmit power will improve the SNR, therefore, the BER is decreased.

The impact of changing the modulation order M on the overall BER is shown in the first sub-figures (*a*) in Fig. 10

- Fig. 17 for all system setups. Both N and σ_o^2 are fixed to $N = 4$ and $\sigma_o^2 = 1°$, respectively, while three different values of the modulation order M are considered $M = 2$, 4 and 8. As expected, in all setups, increasing the modulation order will increase the BER in both hops, which is mainly due to increasing the bits per symbol transmitted each time. The average BER increases as it can be clearly noted in the results.

In the sub-figures (*b*) in Fig. 10 - Fig. 17, the average BER versus the transmit power is plotted at different numbers of antenna' elements for all system setups. Both M and σ_o^2 are fixed to $M = 8$ and $\sigma_o^2 = 1°$, respectively, and three different value of the number of the antenna elements are assumed $N = 4$, 8 and 12. Unlike the impact on the OP, increasing the number of antenna elements N leads to improve the average BER, which is mainly due to increases the received SNR at
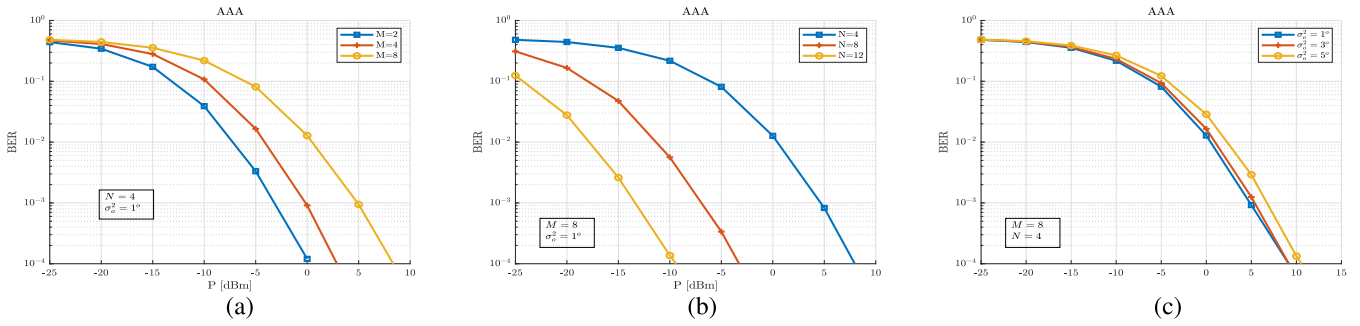
FIGURE 16. The BER of the AAA setup versus the transmit power showing (a) The impact of M (b) The impact of N and (c) The impact of σ_o^2.
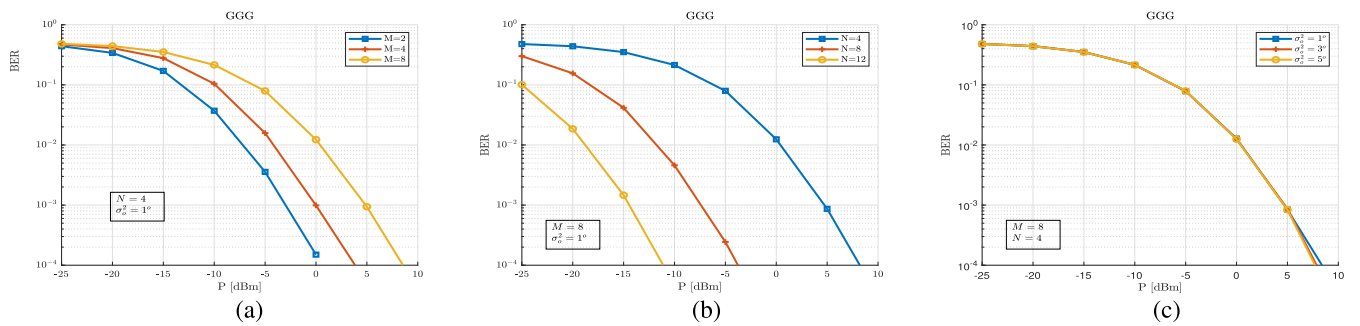

FIGURE 17. The BER of the GGG setup versus the transmit power showing (a) The impact of M (b) The impact of N and (c) The impact of σ_o^2.

the destination resulted from the larger number of antenna elements used.

In the third sub-figures (c) in Fig. 10 - Fig. 17 both M and N are fixed to $M = 8$ and $N = 4$, respectively, where three different values of the vibration intensity $\sigma_o^2 = 1°$, $3°$ and $5°$ are considered. A clear negative impact of increasing the vibration intensity σ_o^2 on the system performance appears, which is mainly due to losing the alignment between antennas due to the UAVs' vibrations.

C. COMPARISON OBSERVATIONS

Although all UAV-assisted setups have a common behaviour of both BER and OP versus any of the investigated operational parameters, they are affected in different extents, and there are some general observations that can be made based on both BER and OP results for all setups considered. First, comparison among all setups reveals that increasing the number of aerial entities degrades the performance in terms of both OP and BER. This is mainly due to the vibrations of the hovering aerial nodes that cannot be eliminated. As mentioned earlier, vibration will directly affect the antennas' orientation, which significantly impacts the received SNR in mmWave-based links. Therefore, it is clear from the OP and BER results that the results of AAA setup has the worst performance as compared to other setup. Also, the results of GGG attain the best performance among all others. Specifically, setups that have one aerial entity (i.e., AGG, GAG, GGA) attain lower outage rate and higher average BER than setups that include two aerial entities (i.e.,

AAG, AGA and GAA). However, one can ask about the reason of including aerial nodes as the performance gets worse. Here, it is worth highlighting that dual-hop UAV-assisted links come to create a link between two nodes that cannot be connected on the ground. Also, the mathematical framework and the results in this study provide a tool for the system designer to evaluate the performance, and hence, select the best system setup.

VI. CONCLUSION

This paper has investigated the performance of dual-hop UAV-assisted mmWave-based links using decode-and-forward protocol. As nodes can be either aerial or ground nodes, eight different system setups, which represent all possible node combinations of UAV-assisted dual-hop links, have been considered and analyzed. The analysis has presented a generalized closed-form expressions for both probability distribution function and cumulative density function of the signal-to-noise ratio for all possible single-hop links (AA, AG, GA and GG), which have been used to formulate the end-to-end OP and the average BER for all proposed setups. Analytical and Monte Carlo simulation results have shown the impacts of the transmit power, the number of antenna elements, the modulation order and the UAV's vibration intensity of on the outage and error performance. This paper offers the possibility of finding the optimal values of the link parameters and provides an extensive reference for engineering practice in the field of UAV-assisted mmWave links.

Extending this work can include analyzing other performance aspects such as channel capacity, secrecy capacity and wireless coverage. Future work may also consider aerial nodes powered by energy harvesting, which can be a interesting extension of this work. Also, employing artificial intelligence tools for optimizing the performance of UAV-assisted links can be investigated in future studies.

REFERENCES

[1] L. Gupta, R. Jain, and G. Vaszkun, "Survey of important issues in UAV communication networks," *IEEE Commun. Surveys Tuts.*, vol. 18, no. 2, pp. 1123–1152, 2nd Quart., 2016.

[2] M. W. Lewis, "Drones and the boundaries of the battlefield," *Texas Int. Law J.*, vol. 47, p. 293, Jan. 2011.

[3] A. Utsav, A. Abhishek, P. Suraj, and R. Kr. Badhai, "An IoT based UAV network for military applications," in *Proc. 6th Int. Conf. Wireless Commun., Signal Process. Netw. (WiSPNET)*, Chennai, India, Mar. 2021, pp. 122–125.

[4] G. Cai, J. Dias, and L. Seneviratne, "A survey of small-scale unmanned aerial vehicles: Recent advances and future development trends," *Unmanned Syst.*, vol. 2, no. 2, pp. 175–199, 2014.

[5] P. S. Ramesh and J. V. Jeyan, "Comparative analysis of the impact of operating parameters on military and civil applications of mini unmanned aerial vehicle (UAV)," in *Proc. AIP Conf.*, 2020, vol. 2311, no. 1, Art. no. 030034.

[6] A. Rovira-Sugranes, A. Razi, F. Afghah, and J. Chakareski, "A review of AI-enabled routing protocols for UAV networks: Trends, challenges, and future outlook," *Ad Hoc Netw.*, vol. 130, May 2022, Art. no. 102790.

[7] F. Noor, M. A. Khan, A. Al-Zahrani, I. Ullah, and K. A. Al-Dhlan, "A review on communications perspective of flying ad-hoc networks: Key enabling wireless technologies, applications, challenges and open research topics," *Drones*, vol. 4, no. 4, p. 65, 2020.

[8] S. A. H. Mohsan, N. Q. H. Othman, Y. Li, M. H. Alsharif, and M. A. Khan, "Unmanned aerial vehicles (UAVs): Practical aspects, applications, open challenges, security issues, and future trends," *Intell. Service Robot.*, vol. 16, no. 1, pp. 109–137, 2023.

[9] S. A. H. Mohsan, M. A. Khan, F. Noor, I. Ullah, and M. H. Alsharif, "Towards the unmanned aerial vehicles (UAVs): A comprehensive review," *Drones*, vol. 6, no. 6, p. 147, Jun. 2022.

[10] A. Iqbal, M. L. Tham, Y. J. Wong, G. Wainer, Y. X. Zhu, and T. Dagiuklas, "Empowering non-terrestrial networks with artificial intelligence: A survey," *IEEE Access*, vol. 11, pp. 100986–101006, 2023.

[11] M. Ghamari, P. Rangel, M. Mehrubeoglu, G. S. Tewolde, and R. S. Sherratt, "Unmanned aerial vehicle communications for civil applications: A review," *IEEE Access*, vol. 10, pp. 102492–102531, 2022.

[12] R. Kovalchukov, D. Moltchanov, A. Samuylov, A. Ometov, S. Andreev, Y. Koucheryavy, and K. Samouylov, "Analyzing effects of directionality and random heights in drone-based mmWave communication," *IEEE Trans. Veh. Technol.*, vol. 67, no. 10, pp. 10064–10069, Oct. 2018.

[13] R. Chataut, M. Nankya, and R. Akl, "6G networks and AI revolution—Exploring technologies, applications, and emerging challenges," *Preprints*, 2023, doi: 10.20944/preprints202312.0829.v1.

[14] N. Rupasinghe, Y. Yapici, I. Güvenç, and Y. Kakishima, "Non-orthogonal multiple access for mmWave drone networks with limited feedback," *IEEE Trans. Commun.*, vol. 67, no. 1, pp. 762–777, Jan. 2019.

[15] N. Zhao, W. Lu, M. Sheng, Y. Chen, J. Tang, F. R. Yu, and K.-K. Wong, "UAV-assisted emergency networks in disasters," *IEEE Wireless Commun.*, vol. 26, no. 1, pp. 45–51, Feb. 2019.

[16] H. Qu, W. Zhang, J. Zhao, Z. Luan, and C. Chang, "Rapid deployment of UAVs based on bandwidth resources in emergency scenarios," in *Proc. Inf. Commun. Technol. Conf. (ICTC)*, Nanjing, China, May 2020, pp. 86–90.

[17] R. Al-Khatab, S. Althunibat, A. Alhasanat, and K. Qaraqe, "Outage analysis of dual-hop UAV-assisted links considering orientation fluctuations," in *Proc. 6th Int. Conf. Adv. Commun. Technol. Netw. (CommNet)*, Rabat, Morocco, Dec. 2023, pp. 1–8.

[18] W. Khawaja, O. Ozdemir, and I. Guvenc, "UAV air-to-ground channel characterization for mmWave systems," in *Proc. IEEE 86th Veh. Technol. Conf. (VTC-Fall)*, Toronto, ON, Canada, Sep. 2017, pp. 1–5.

[19] W. Khawaja, O. Ozdemir, F. Erden, I. Guvenc, and D. W. Matolak, "UWB air-to-ground propagation channel measurements and modeling using UAVs," in *Proc. IEEE Aerosp. Conf.*, Big Sky, MT, USA, Mar. 2019, pp. 1–10.

[20] W. Khawaja, O. Ozdemir, and I. Guvenc, "Channel prediction for mmWave ground-to-air propagation under blockage," *IEEE Antennas Wireless Propag. Lett.*, vol. 20, pp. 1364–1368, 2021.

[21] N. Goddemeier and C. Wietfeld, "Investigation of air-to-air channel characteristics and a UAV specific extension to the Rice model," in *Proc. IEEE Globecom Workshops (GC Wkshps)*, San Diego, CA, USA, Dec. 2015, pp. 1–5.

[22] J. Shucong and L. Zhang, "Modelling unmanned aerial vehicles base station in ground-to-air cooperative networks," *IET Commun.*, vol. 11, no. 8, pp. 1187–1194, 2017.

[23] B. Shen, J. Chen, G. Xu, Q. Chen, and J. Wang, "Performance analysis of a drone-assisted FSO communication system over Málaga turbulence under AoA fluctuations," *Drones*, vol. 7, no. 6, p. 374, Jun. 2023.

[24] A. A. Khuwaja, Y. Chen, N. Zhao, M.-S. Alouini, and P. Dobbins, "A survey of channel modeling for UAV communications," *IEEE Commun. Surveys Tuts.*, vol. 20, no. 4, pp. 2804–2821, 4th Quart., 2018.

[25] G. Xu, N. Zhang, M. Xu, Z. Xu, Q. Zhang, and Z. Song, "Outage probability and average BER of UAV-assisted dual-hop FSO communication with amplify-and-forward relaying," *IEEE Trans. Veh. Technol.*, vol. 72, no. 7, pp. 8287–8302, Jul. 2023.

[26] J. Wang, G. Xu, Z. Zhao, M. Xu, X. Yu, and Q. Zhang, "Performance analysis of dual-hop UAV-assisted FSO communication system with DF protocol," in *Proc. 14th Int. Conf. Wireless Commun. Signal Process. (WCSP)*, Nanjing, China, Nov. 2022, pp. 900–904.

[27] J.-Y. Wang, Y. Ma, R.-R. Lu, J.-B. Wang, M. Lin, and J. Cheng, "Hovering UAV-based FSO communications: Channel modelling, performance analysis, and parameter optimization," *IEEE J. Sel. Areas Commun.*, vol. 39, no. 10, pp. 2946–2959, Oct. 2021.

[28] L. Kong, L. Ye, F. Wu, M. Tao, G. Chen, and A. V. Vasilakos, "Autonomous relay for millimeter-wave wireless communications," *IEEE J. Sel. Areas Commun.*, vol. 35, no. 9, pp. 2127–2136, Sep. 2017.

[29] L. Zhu, J. Zhang, Z. Xiao, X. Cao, X.-G. Xia, and R. Schober, "Millimeter-wave full-duplex UAV relay: Joint positioning, beamforming, and power control," *IEEE J. Sel. Areas Commun.*, vol. 38, no. 9, pp. 2057–2073, Sep. 2020.

[30] H. Ajam, M. Najafi, V. Jamali, and R. Schober, "Ergodic sum rate analysis of UAV-based relay networks with mixed RF-FSO channels," *IEEE Open J. Commun. Soc.*, vol. 1, pp. 164–178, 2020.

[31] M. T. Dabiri, M. Rezaee, V. Yazdanian, B. Maham, W. Saad, and C. S. Hong, "3D channel characterization and performance analysis of UAV-assisted millimeter wave links," *IEEE Trans. Wireless Commun.*, vol. 20, no. 1, pp. 110–125, Jan. 2021.

[32] *Study on Channel Model for Frequencies From 0.5 to 100 GHz (Release14)*, document 3GPP TR 38.901 V14.1.1, Jul. 2017.

[33] *Technical Specification Group Radio Access Network; Study of Radio Frequency (RF) and Electromagnetic Compatibility (EMC) Requirements for Active Antenna Array System (AAS) Base Station*, document 37.840, 3GPP TR, 2013.

[34] C. A. Balanis, *Antenna Theory: Analysis and Design*. Hoboken, NJ, USA: Wiley, 2016.

[35] A. Papoulis and S. U. Pillai. *Probability, Random Variables and Stochastic Processes*. New York, NY, USA: McGraw-Hill, 2002.

[36] O. S. Badarneh and R. Mesleh, "Diversity analysis of simultaneous mmWave and free-space-optical transmission over *F*-distribution channel models," *J. Opt. Commun. Netw.*, vol. 12, no. 11, pp. 324–334, Nov. 2020.

[37] E. W. Ng and M. Geller, "A table of integrals of the error functions," *J. Res. Nat. Bureau Standards B*, vol. 73, no. 1, pp. 1–20, Jan./Mar. 1969.
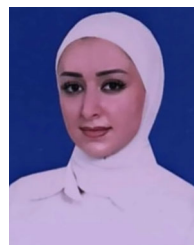
RAYYAN AL-KHATAB received the B.Sc. degree in electrical engineering from Al-Hussein Bin Talal University, Jordan, in 2020, where she is currently pursuing the M.Sc. degree in computer and network engineering. Her research interests include cooperative networks, relaying techniques, unmanned aerial vehicles, and performance analysis of communication systems.

SAUD ALTHUNIBAT (Senior Member, IEEE) received the Ph.D. degree in telecommunications from the University of Trento, Trento, Italy, in 2014. He is currently a Professor with Al-Hussein Bin Talal University, Ma'an, Jordan. He has authored more than 150 scientific articles. His research interests include a wide range of wireless communication topics, such as index modulation, spectrum sharing, cognitive radio, wireless sensor networks, energy efficiency, and resource allocation. He was a recipient of the Best Paper Awards in IEEE CAMAD 2012 and IEEE Globecom 2022. He was also a recipient of the Distinguished Researcher Award granted by the Hamdi Mango Center, The University of Jordan, in 2022. He is the General Co-Chair of BROADNETs 2018 Conference. He was selected as an Exemplary Reviewer of the IEEE Communications Letters, in 2013. He serves as an Editor for the IEEE Communications Letters.

ABDULLAH ALHASANAT (Member, IEEE) received the B.Sc. degree in computer engineering from the University of Aden, Yemen, in 2004, the M.Sc. degree in computer engineering from Jordan University of Science and Technology, Jordan, in 2007, and the Ph.D. degree in wireless networks from the University of Newcastle, U.K., in 2012. Currently, he is a Professor of computer engineering with Al-Hussein Bin Talal University, Jordan. He has authored more than 40 papers in high-level scientific journals and international conferences. His main research interests include data gathering in IoT and 5G communication and beyond technologies. In addition, he is also interested in artificial intelligence, machine learning, and computer vision.

KHALID A. QARAQE (Senior Member, IEEE) was born in Bethlehem. He received the B.S. degree (Hons.) from the University of Technology, Baghdad, Iraq, in 1986, the M.S. degree from The University of Jordan, Amman, Jordan, in 1989, and the Ph.D. degree from Texas A&M University, College Station, TX, USA, in 1997, all in electrical engineering. From 1989 to 2004, he has held a various positions with many companies. He has over 12 years of experience in telecommunication industry. He has worked on numerous projects and has experience in product development, design, deployments, testing, and integration. He joined the Department of Electrical and Computer Engineering, Texas A&M University at Qatar, in July 2004, where he is currently a Professor and the Managing Director with the Center for Remote Healthcare Technology, Qatar. He has been awarded more than 20 research projects consisting of more than USD 13M from local industries in Qatar and Qatar National Research Foundation (QNRF). He has published more than 131 journal articles in top IEEE journals and published and presented 250 papers at prestigious international conferences. He has 20 book chapters published, four books, three patents, and presented several tutorials and talks. His research interests include communication theory and its application to design and performance, analysis of cellular systems, and indoor communication systems, particularly mobile networks, broadband wireless access, cooperative networks, cognitive radio, diversity techniques, index modulation, visible light communication, FSO, tele-health, and noninvasive bio sensors. He received the Itochu Professorship Award, from 2013 to 2015; the Best Researcher Award from QNRF, in 2013; the Best Paper Award from the IEEE First Workshop on Smart Grid and Renewable Energy, in 2015; the Best Paper Award from the IEEE Globecom, in 2014; the Best Poster Award at IEEE Dyspan Conference, in 2012; the TAMUQ Research Excellence Award, in 2010; the Best Paper Award from ComNet, in 2010; the Best Paper Award from CROWNCOM, in 2009; the Best Paper Award from ICSPC'0, in 2007; the *IEEE Signal Processing Magazine* Best Column Award, in 2018; the Best Oral Presentation Award from CECNet, in 2018; the Best Paper Award at Green Communications, Computing and Technologies Conference, in 2016; the Faculty of the Year (Student Award), in 2016 and 2015, respectively; and the Best Faculty Award by the Student Body, in 2015.

• • •